analytical chemistry

Article

Cite This: Anal. Chem. XXXX, XXX, XXX−XXX

pubs.acs.org/ac

A Universal Electrochemical Biosensor Using Nick-HCR Nanostructure as Molecular Gate of Nanochannel for Detecting Chromium(III) Ions and MicroRNA

Longjiao Zhu,[†,‡] Miao Miao,[†,‡] Xiangli Shao,[†,‡] Zaihui Du,[†,‡] Kunlun Huang,[†,‡,§] Yunbo Luo,[†,‡] and Wentao Xu*[,†,‡,§]

[†]Beijing Advanced Innovation Center for Food Nutrition and Human Health, College of Food Science & Nutritional Engineering, China Agricultural University, Beijing 100083, P. R. China

[‡]Key Laboratory of Safety Assessment of Genetically Modified Organism (Food Safety), Ministry of Agriculture, Beijing 100083, P.R. China

[§]Beijing Laboratory for Food Quality and Safety, College of Food Science and Nutritional Engineering, China Agricultural University, Beijing 100083, P. R. China

Supporting Information

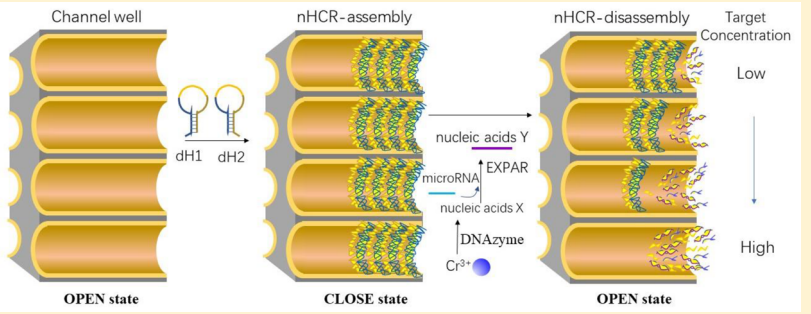

ABSTRACT: Solid-state nanochannels demonstrating excellent mechanical properties and chemical stability combined with programmable DNA provide an opportunity to control on-demand ion transport. However, poor functionalization of the nanochannels limits the types of detected targets, as well as its universality in the sensing field. To solve these issues, a universal nanochannel sensing platform was developed by employing a nick hybridization chain reaction (nHCR) nanostructure as a molecular gate, which could generally respond to the universal sequence Y. Metal ion-dependent DNAzyme cleavage was used to transfer the chromium(III) (Cr^{3+}) ions into nucleic acid X, which was further amplified and converted into universal sequence Y. Upon adding sequence Y into the nHCR nanostructure-functionalized nanochannel, the disassembly of the nHCR molecular gate turned on the ionic current signal inside the nanochannel. The ON−OFF ratio displayed a linear relationship with the Cr^{3+} concentration in the range from 200 fM to 20 nM. In less than 66 min, the nanochannel-based biosensing platform successfully detected Cr^{3+} ions as low as 200 fM. In addition, the detection of microRNA with a concentration as low as 1 pM was achieved by only regulating the sequence of template X′−Y′.

The gating of biological nanochannels, which generally respond to physiological stimuli by switching the nanochannel between CLOSED and OPEN states, is a common biological phenomenon in organisms. Inspired by the biological gating nature, the development of artificial nanofluidic gating systems being able to perform analytical functions have attracted ever-increasing attention.[1] The combination of biomolecules with solid-state nanochannels allows for the development of a nanofluidic gating and smart bioinspired device,[2] as well as biosensing devices in confined nanoscale.[3,4] The nanoscale bioanalytical system has attracted increasing interest since the system can handle fast chemical reactions, allow for batch fabrication and miniaturization, and result in low manufacturing costs. A representative synthetic nanochannel is anodized aluminum oxide (AAO) porous membranes, whose high channel density and small diameters result in AAO with an extensive surface area that can easily be functionalized. Biomolecule-functionalized nanochannels have been successfully applied in the detection of Pb (II),[5] DNA,[6] telomerase activity,[7] biomolecular recognition events,[8] and protein.[9] The Li group also reported on a rhodopsin-like ionic gate fabricated with graphene oxide and an isomeric DNA switch for the photocontrol of ion transport.[10] In these applications, the synthetic nanochannel provides reliable support, while biomolecules or chemical moieties act as capture probes.[11] Furthermore, the signal output mainly

Received: July 31, 2019
Accepted: October 7, 2019
Published: October 7, 2019

DOI: 10.1021/acs.analchem.9b03489
Anal. Chem. XXXX, XXX, XXX−XXX

depends on monitoring the change in ion transport through the binding of the event-induced nanochannel gating. Despite its excellent analytical performance, one limitation is that a nanochannel grafted with a particular molecule probe can only be used for sensing a particular substance. To detect different analytes, it is necessary to prepare a different probe-functionalized nanochannel, which is time consuming and inconvenient. Moreover, the regeneration of the nanochannel functionality may be impeded by further tedious modifications. To overcome these challenges, an alternative "probe" is proposed.

The programmability makes DNA a fascinating, multifunctional material for fabricating super nanostructures in nanoscale.[12] In recent years, impressive progress has been made in the construction of DNA-based super nanostructures. In 2004, Dirks and Pierce programmatically designed two metastable hairpins, with partially overlapped complementarities to generate a long double-stranded DNA with a super nanostructure after adding an initiator DNA.[13] The super nanostructures were fabricated using structure-dependent DNA self-assembly nanotechnology, known as HCR. HCR appears to be appealing due to its isothermal amplification, simple protocol,and enzyme-free nature.[14] Furthermore, HCR is widely applied in bioanalytical systems, such as paper-based biosensors,[15] colorimetric assays,[16,17] electrochemical assays,[18−20] bioluminescent assays,[21] and fluorescent assays.[22−24] However, these bioanalytical systems depend on a particular sequence and are, therefore, only suitable for one specific nucleic acid target. Therefore, to expand the range of detection targets, the aptamer was integrated with the HCR nanostructure to construct switchable concatemers for the detection of both Ochratoxin A and microRNA. The switchable concatemers provided an ideal molecular gating material with a molecular weight exceeding 1500 base pairs (bp). However, a significant challenge remains, in that considerable target input is required to dismantle the aptamer from the HCR nanostructures, resulting in low analytical sensitivity of the non-nucleic acid targets.

To solve the above problems, a new easily-disassemble nick-HCR nanostructure was designed by inserting a universal ssDNA in the HCR hairpins to form the nick labelled long dsDNA nanostructure. The nick can hybridize with the universal probe Y (ssDNA), resulting in the collapse of the super nanostructure. After the nanochannel is functionalized with the easily detachable nick hybridization chain reaction (nHCR) nanostructure, a new nanofluidic gating system is fabricated for the response of universal probe Y. Furthermore, to obtain detection universality of the nanofluidic gating system, it is necessary for some transit systems to convert the target analytes into universal probe Y. The exponential amplification reaction (EXPAR) is extraordinary technology employed for the amplification of nucleic acids and can provide a cycle reaction system between polymerase strand extension and single-strand nicking at 55 °C. The reaction amplifies short oligonucleotides 10^6-10^9 fold under isothermal conditions within 15 min.[25] In addition, EXPAR has remarkable capabilities regarding nucleic acid sequence transformation and can be achieved by designing template chain sequences. Therefore, EXPAR is employed in this research to transform specific nucleic acids analytes into universal probe Y. MicroRNAs with vital biological regulatory significance[26] and cancer correlation[27] were selected as specific nucleic acid model targets.

The Cr^{3+} ion is a well-known mutagen and carcinogen. Moreover, it is a bioaccumulative metal ion that cannot be disposed of by the body and can, therefore, lead to tissue damage,[28] as well as human cells damage.[29] In addition, recent studies indicated that Cr^{3+} ions inhibit some enzymes while deactivating essential cellular pathways,[30] necessitating constant monitoring of the levels of Cr^{3+} ions in the living body or environment. Therefore, the Cr^{3+} ion is selected as the non-nucleic acidmode analyte in this paper. To further achieve the detection of non-nucleic acid targets, an easily synthesized, highly stable, and cost-effective Ce13d metal ion enzyme[29,31] was also used to transfer Cr^{3+} ions to the nucleic acid signal.[32]

This study demonstrates a nanochannel electrochemical biosensor fabricated via an nHCR nanostructure, which is easily detachable while exhibiting an excellent switch ratio and exceptional dual-target responsiveness.

EXPERIMENTAL SECTION

Reagents. Cr^{3+} and other metal salts were purchased from Sigma-Aldrich (Shanghai, China). SYBR Green I (10000×) was purchased from the Beijing Solarbio Science & Technology Co., Ltd. (Beijing, China). The AAO porous membranes were purchased from Hefei Puyuan Nanotechnology Co., Ltd. (Hefei, China). Tris(hydroxymethyl)-aminomethane (Tris, 99%) was purchased from Amersco (Shanghai, China). (3-Aminopropyl) trimethoxysilane (APS, 97%) and the glutaraldehyde solution (25% in H_2O) were purchased from Sigma-Aldrich (Shanghai, China). The DNA sequences used in this paper were synthesized at Invitrogen (Shanghai, China).

Bst DNA polymerase and Nt.BstNBI nicking endonuclease were purchased from New England Biolabs (Beijing, China). The D2000 standard molecular weight DNA (MD114) was purchased from Tiangen Biotechnology Co., Ltd. (Beijing, China). Deoxyribonucleotide triphosphates (dNTPs) were purchased from Takara Biotechnology Co., Ltd. The ultrapure water was homemade in the laboratory using a Millipore Milli-XQ purification apparatus (Bedford, USA).

Apparatus. The Keithley 2638 picoammeter/voltage source was purchased from Tektronix, Inc. (Washington, USA). The BIO-RAD iCycler Thermal Cycler W/iQ5 Optical Module was used for real-time PCR (RT-PCR). The gel imaging and analysis were accomplished using the GenoSens 1850 Gel Imager, which was purchased from Junyue Co., Ltd.

Transform Procedures Performed Outside the Nanochannel. The catalytic strand (40 nM) and substrate strand (80 nM) were mixed in 50 μL of cutting buffer (50 mM MES, 25 mM NaCl, 0.8 mM phosphate, pH 6.0) and heated at 95 °C for 15 min, after which it was gradually cooled to 25 °C where it was incubated for 3 min. The Cr^{3+} solution with a specific concentration was added, and the sample was incubated at 28 °C for 30 min. Finally, the reaction was terminated with 25 mM EDTA. The cutting products were characterized by 20% denaturing polyacrylamide gel electrophoresis (dGE) at 120 V for 2 h.

The EXPAR reactions were performed at 55 °C in two separate parts. Part A utilized 1× Nt.BstNBI buffer 3.1, 1× ThermoPol buffer, dNTPs (0.5 μM), 1× SYBR Green I, amplification template X′−Y′ (80 nM) and Y′−Y′ (20 nM), ultrapure water, and DNA X from the DNAzyme cutting products. Part B consisted of Nt.BstNBI nicking endonuclease (0.2 U/μL), Bst. DNA polymerase (0.04 U/μL), and ultrapure water. The total reaction volume was 50 μL. The real-time

DOI: 10.1021/acs.analchem.9b03489
Anal. Chem. XXXX, XXX, XXX−XXX

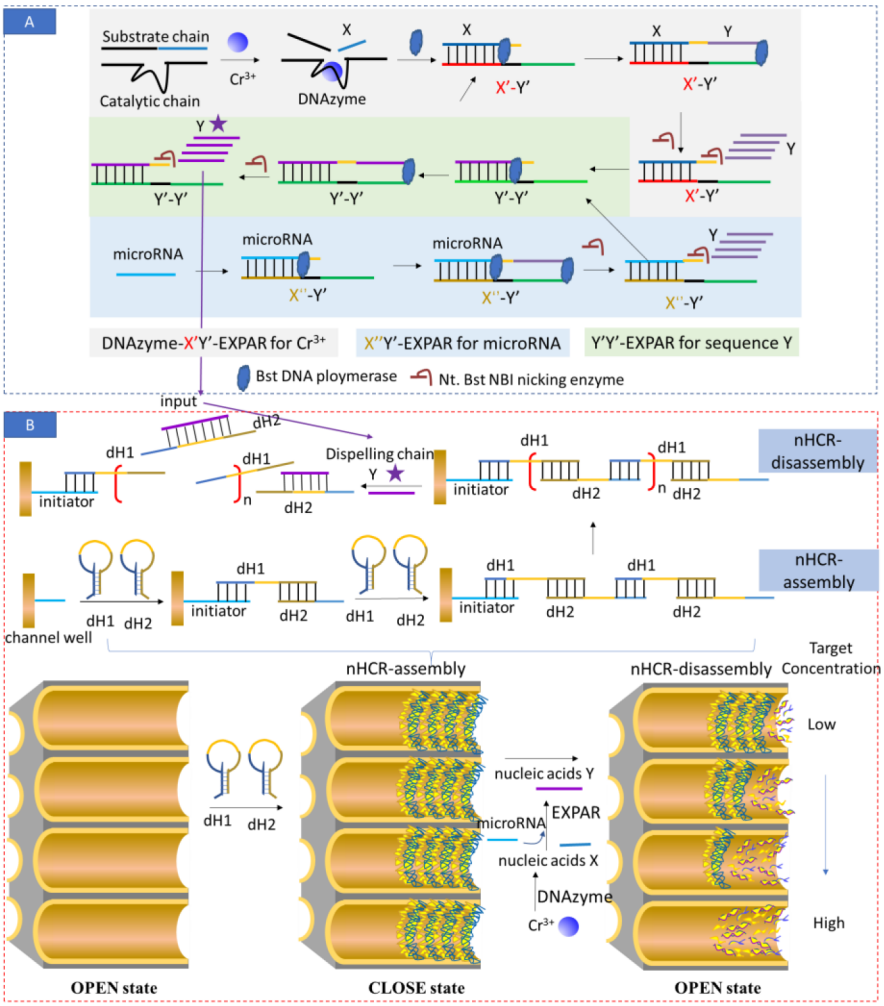

Figure 1. Schematic illustration of the fabricated nanofluidic gating biosensor. (A) Cr^{3+} transformation and enrichment were performed outside the nanochannel using the Cr^{3+} -responsive cleavage DNAzyme and the dual exponential amplification reaction (dEXPAR). MicroRNA can directly be converted into sequence Y using the dEXPAR system with template X′′-Y′ and Y′-Y′. (B) Assembly and disassembly of nHCR nanostructures inside nanochannel.

fluorescence intensity was monitored at 4 s intervals after the A and B mixtures were placed in the BIO-RAD quantitative PCR.

Feasibility Analysis of Assembly and Disassembly of nHCR Nanostructures in Liquid Phase. The nHCR reaction was initiated by mixing 10 nM initiator DNA with 100 nM dH_1 and 100 nM dH_2 in the nHCR buffer, followed by incubation at 37 °C for 60 min. Furthermore, the dispelling ssDNA Y was added to the nHCR product solution and incubated at 37 °C for 30 min. Then, 10 μL of each product was subjected to gel electrophoresis on 2% agarose gel at 130 V for 25 min. Images were captured using the GenoSens 1850 Gel Imager.

Fabrication of nHCR Nanostructure-Functionalized Nanochannels. To construct the nick-HCR assembly gated nanochannel sensor, the nanochannel with a diameter of 80−100 nm with optimal topological morphology and channel density was selected as the solid nanomaterial for fabricating sensors. The previously reported glutaraldehyde method was integrated with an air-column method for asymmetric functionalization of the nanochannel. Then 1 μM nucleic acid is used as the minimum effective concentration for construction of molecular gates. The detail construction protocol is as follows: Cleaned alumina membranes containing bared nanochannels were first immersed in 20 mL of a 7.5% acetone solution containing APS and incubated at 28 °C for 2 h. After being thoroughly washed in acetone, the membranes were dried in an oven at 78 °C for 2 h. To immobilize the aminated capture probe (initiator DNA) asymmetrically onto the alumina surface, half of the membranes were immersed overnight in a 25% glutaraldehyde solution at 28 °C overnight. After that, the asymmetric modified membranes were immersed in 5′-aminated initiator DNA (1 μM) in a Tris-HCl solution (1 mM $MgCl_2$, 500 mM NaCl, pH 7.4) for 6 h. After rinsing three times with water, 1 μM dH_1 and 1 μM dH_2 were added to the initiator-mobilized membranes in the nHCR buffer (2.5 mM NaH_2PO_4, 8.0 mM Na_2HPO_4, 0.15 mM NaCl, and 2.0 mM $MgCl_2$, pH 7.4) at 28 °C overnight and then washed with water before performing the electrical measurements.

Disassembly of nHCR Nanostructure-Functionalized Nanochannels. For Cr^{3+} ion detection, the nHCR nanostructure-modified nanochannels were immersed in the DNAzyme−dEXPAR product solution, which contained the transferred sequence Y. For microRNA detection, the nano-

DOI: 10.1021/acs.analchem.9b03489
Anal. Chem. XXXX, XXX, XXX−XXX

channels gated with nHCR nanostructures were immersed in the dEXPAR product solution, which also contained the transferred sequence Y. It should be mentioned that the template sequence used in the dEXPAR system was different from that of Cr^{3+}. The microRNA directly complementary with X′′ initiated X′′Y′-EXPAR and Y′Y′-EXPAR without the requirement of preconversion assisted by DNAzyme. The disassembly was performed in an nHCR buffer. The formation of nHCR nanostructures was demonstrated by agarose gel electrophoresis, while the modification of the nHCR nanostructures on the membrane surface was characterized using scanning electron microscopy (SEM) observation, and the modification of the nHCR nanostructures inside the nanochannel was characterized using laser scanning confocal microscopy (LSCM).

Electrical Measurements of the Transmembrane Ionic Current. To study conductivity and gating properties, the unmodified or nHCR nanostructure-modified AAO membrane with a measured area of about 0.7−1 mm^2 was placed between two electrolyte solution storage cells. The transmembrane ionic current of the treated nanochannels was measured with Ag/AgCl electrodes using a Keithley 2638 picoammeter/voltage source. The main transmembrane potential was a sweep voltage from −2 V to +2 V with an interval of 100 s. The electrolyte used in the electrical measurement was 10 mM KCl solution (pH 5.8).

RESULTS AND DISCUSSION

Principle of Nanochannel Biosensor for Detection of Cr^{3+} or MicroRNA. A universal nanochannel biosensing system for the detection of Cr^{3+} ions was developed using DNAzyme and EXPAR for target transformation and amplification and an easily detachable nHCR nanostructure-functionalized nanochannel for signal output. Figure 1 illustrates the detailed biosensing principle of the nanochannel biosensor.

In the constructed nanochannel biosensor, model analyte Cr^{3+} ions activated the cutting activity of the Ce13d cleavage DNAzyme, transforming Cr^{3+} into transient sequence X. Then, the freed sequence X served as the boot sequence of the EXPAR to transform it into an accumulated universal sequence Y. A dual exponential amplification reaction (dEXPAR) strategy was used, which is schematically illustrated in Figure 1A. To initiate the EXPAR, a primer-template was formed and initiated by the Bst DNA polymerase for DNA elongation along the template X′-Y′ in the presence of dNTPs. Then, the Nt.BstNBI nicking endonuclease cleaved synthetic DNA strands X-Y at the nicking point, recreating a primer-template for initiating the next round of DNA elongation. Consequently, the newly synthesized oligonucleotide Y complementary with the template beyond the nicking site was dissociated and used as a new primer to initiate a template Y′-Y′-assisted EXPAR. After X′Y′-EXPAR and Y′Y′-EXPAR, the Cr^{3+} ions were exponentially transformed into universal nucleic acid sequence Y at 55 °C.

Finally, the accumulated sequences Y were input into the nHCR nanostructure asymmetrically functionalized nanochannels, triggering a chain displacement-induced disassembly of the nHCR nanostructures. As a result, the nanochannels transformed from a CLOSED state to an OPEN state, and the transmembrane ionic current displayed a sharp increase (Figure 1B). Moreover, Cr^{3+} was determined by monitoring the changes in the transmembrane ionic current. It should be mentioned that the CLOSED state of the nanochannel was prefabricated by successive, asymmetrical chemical modification and the covalent coupling of the amino-carbonyl group and hybridization chain reaction of two fuel hairpins (Figure 1B, nHCR-assembly). The prefabrication of nHCR nanostructures in the nanochannel allowed for the generation of signals in one step by using target transformed universal sequence Y for the direct digestion of the nHCR nanostructure. In addition, the microRNAs could be detected by simply regulating the template X′-Y′ into the template X′′Y′ in the dEXPAR process.

In this paper, the Cr^{3+} ions and microRNAs were successfully determined by measuring the changes in the transmembrane ionic current. The sequences used in the nanochannel biosensor are listed in Table S2.

Nick Hybridization Chain Reaction (nHCR). The flexible, super nanostructures and programmability make HCR products a favorable nanomaterial for the fabrication of a molecular gate. Furthermore, the isothermal and enzyme-free assembly properties allow HCR to be applied in the biosensing field for the analysis of various targets, such as Hg^{2+},[33] biomolecules,[34] and DNA.[35] However, due to the sequence stringency of HCR, different hairpins were required for different targets in the resultant biosensor. To further enhance the generality, a universal sequence (G-rich sequence) was inserted into the loop section of the hairpins to remold the dH2. In the presence of initiator DNA, the dH1 and dH2 were cascade hybridized through toehold-mediated strand displacement. However, the universal sequence inserted in dH1 and dH2 does not provide energy to drive the hybridization event of HCR because of it being noncomplementary, forming a wide ssDNA nick. The energy storage in the universal sequence was specifically intended for the disassembly of nHCR nanostructures by inputting a dispelling probe Y, which was complementary to the universal sequence. It should be mentioned that the nHCR assembly was more efficient after the insertion of the universal sequence in the hairpins and could be equipped with a long nHCR nanostructure within 1 h. As shown in Figure 2A, typical nHCR products with ladder bands were observed in lanes 2 and 3 when dH_1 and dH_2 were 100 and 100 nM, respectively, while the initiator was 10 nM, and incubated at room temperature for 1 h. The analysis shows that the different lengths of dsDNA consisted of the nHCR products, and the maximum lengths approached approximately 2000 bp. To disassemble the concatenated nHCR nanostructures, three dispelling probes Y (detailed sequences are listed in Table S2) were designed to dismantle the nHCR nanostructures into short DNA fragments. The disassembly of the nHCR products was confirmed by the agarose gel electrophoresis. Notably, probe Y_2 showed a higher disassembly function toward nHCR nanostructures than probes Y_1 and Y_3 (Figure 2A). Moreover, the amount of the dissolved product was proportional to the concentration of the dispelling probe Y (Figure S2), and the optimal digestion time was 30 min (Figure S3). Scanning electron microscopy (SEM) was used to verify the successful assembly and disassembly of nHCR nanostructures on the surface of the AAO membrane. As shown in Figure 2B, after asymmetric chemical modification, the covalent coupling of the amino-carbonyl group, and HCR, a dsDNA film was formed that wrapped the orifices of the nanochannels (Figure 2B-b). The DNA films covering the membrane were primarily destroyed following treatment with probe Y_2 (Figure 2B-c). The LSCM measure-

DOI: 10.1021/acs.analchem.9b03489
Anal. Chem. XXXX, XXX, XXX−XXX

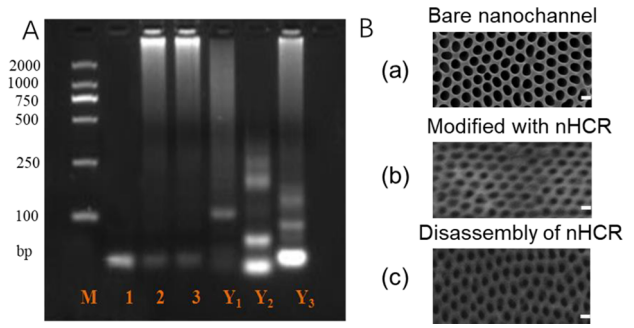

Figure 2. (A) Electrophoresis characterization of the assembly and disassembly of nHCR nanostructures. The assembly conditions of nHCR: Lane 1:100 nM dH_1 + 100 nM dH_2; Lanes 2 and 3: 10 nM initiator + 100 nM dH_1 + 100 nM dH_2; Lanes Y1, Y2, and Y3:10 nM initiator + 100 nM dH_1 + 100 nM dH_2 + 1 μM Y1 or + 1 μM Y2 or + 1 μM Y3 was 1 μM. The assembly and disassembly of nHCR proceeds in nHCR buffer at 25 °C for 60 and 30 min, respectively. (B) SEM characterizations of the assembly and disassembly of the nHCR nanostructure on the membrane surface: (a) bare nanochannels, (b) SEM image of the nHCR nanostructures functionalized porous membrane, (c) after treatment with 1 μM dispelling sequence Y, the SEM image of the porous membrane. The scale bar in the SEM images is 100 nm.

ment was also used to monitor the condition of the DNA assembly or disassembly inside the nanochannels. Assisted by the fluorescence label of the hairpin, it was evident that the fluorescence partially filled the nanochannel, while the thickness of the cross-section fluorescence was approximately half of the nanoporous alumina membranes. After dispelling sequence Y treatment, the fluorescence intensity decreased significantly, displaying a weak fluorescence residue (Figure S4). The LSCM measurement further proved that the assembly and disassembly of nHCR occurred inside the nanochannels.

Characterization and Optimization of the Target Transformation System. The amplification performance of EXPAR and the cleavage event of the Cr^{3+}-responsive DNAzyme were characterized using real-time PCR (RT-PCR) and agarose electrophoresis, respectively. For non-nucleic acid targets, DNAzyme was used to transform Cr^{3+} into transit signal sequence X. The cleavage activity of DNAzyme was verified with 20% dPAGE. As shown in Figure 3A-a, lane 1 was the catalytic chain and lane 2 was the substrate chain, while lanes 7 and 8 were the two synthetic standard cut product chains. Lanes 3, 4, 5, and 6 represented the cutting product following the addition of the Cr^{3+} ion to the gradient concentration, while the cut products were consistent with those of the synthetic standard cut product chains. Although the amount of cutting products increased in conjunction with a higher Cr^{3+} ion concentration, the cutting efficiency cannot meet the analytical requirements. EXPAR is an efficient single-stranded nucleic acid amplification technique that can be performed at a constant temperature. RT-PCR was employed to investigate the feasibility and optimal parameters of the DNAzyme−dEXPAR transformation platform. The Cr^{3+} ions were incubated in advance with DNAzyme, after which the reaction elements of dEXPAR were added in turn to achieve a real-time EXPAR reaction after the cutting process. As shown in Figure 3A-b, the fluorescence signals increased significantly after a 20 min incubation and reached a plateau after being

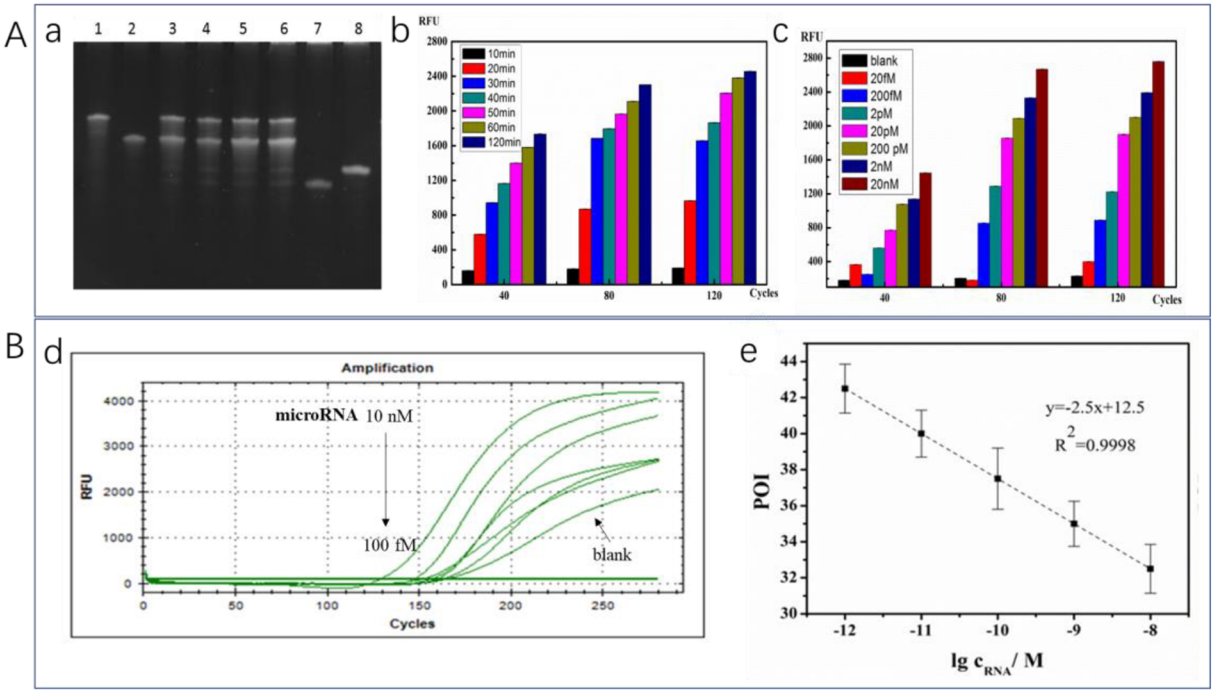

Figure 3. (A) Characterization of the Cr^{3+} transformation effect of the DNAzyme−dEXPAR system using gel electrophoresis and real-time EXPAR. (a) Cleavage activity of Ce13d DNAzyme characterized by 20% dPAGE gel. (b) Optimization of incubation time between Cr^{3+} and Ce13d DNAzyme using real-time EXPAR. (c) The concentration response of the DNAzyme−dEXPAR system was validated by the addition of gradient concentrations of Cr^{3+} from 20 fM to 20 nM. (B) Characterization of the microRNA transformation effect of the dEXPAR′ system using real-time EXPAR. Amplification curve (d) and calibration plot (e) of real-time fluorescence EXPAR in the presence of 100 fM to 10 nM microRNA.

DOI: 10.1021/acs.analchem.9b03489
Anal. Chem. XXXX, XXX, XXX−XXX

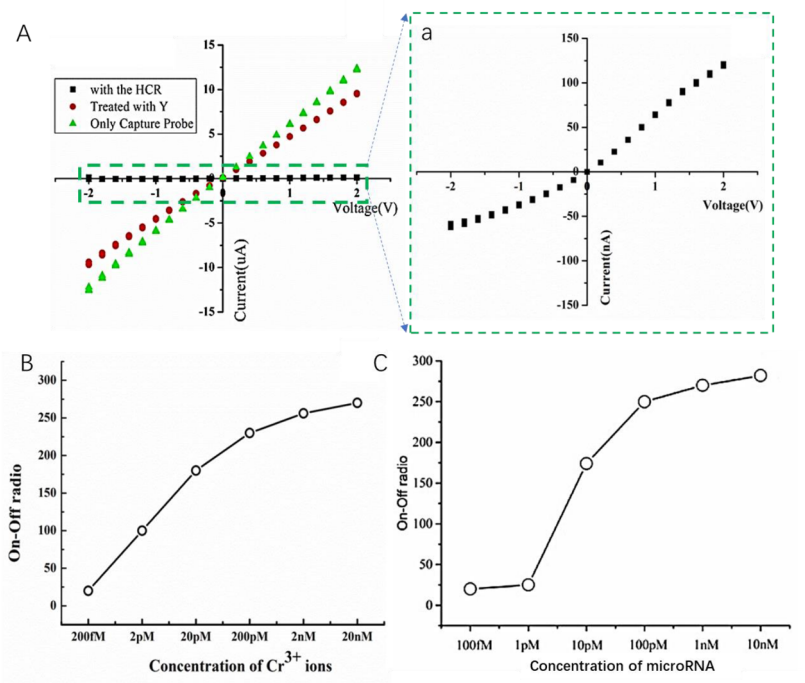

Figure 4. (A) Current−voltage curves of the nanochannel with different treatments; inset (a) indicates that the current−voltage curve of the nanochannels, which was asymmetrically modified with nHCR nanostructures (measured at ±2 V), showed a typical ionic rectification. (B) Analytical performance of the fabricated nanochannel biosensor for Cr^{3+}. (C) Analytical performance of the fabricated nanochannel biosensor for microRNA.

incubated for 30 min. In addition, the fluorescence signals reached a maximum at cycle 80 and then attained an equilibrium, which possibly illustrated that the apocoptic single-stranded X was fully bonded to the template and was saturated. The effective incubation time of Cr^{3+}-DNAzyme was 30 min, while the time of EXPAR was approximately 6 min (80 cycles, each cycle takes 4 s). In summary, the optical transformation times of Cr^{3+} and microRNA are 36 and 6 min, respectively.

Moreover, 20 fM to 20 nM Cr^{3+} was added into the DNAzyme−dEXPAR platform to determine the linear response concentration range. As shown in Figure 3A-c, an excellent linear response was apparent between the fluorescence signal and Cr^{3+} ion concentration at 200 fM and 20 nM. After changing template X′-Y′ into X′-Y′, the microRNA was also successfully detected in the range from 100 fM to 10 nM (Figure 3B-d and B-e). Finally, it was concluded that both the DNAzyme−dEXPAR (for Cr^{3+}) and the dEXPAR′ (for microRNA) system could quantitatively transform the target into universal probe Y.

Feasibility and Analytical Performance of the Nanochannel Sensor. The significant change in the filling state of the nanochannel caused by the assembly and the probe Y-driven disassembly of the nHCR nanostructure inside the nanochannel led to a highly efficient ON−OFF gating system of the electrolyte ions. As shown in Figure 4A, the immobilization of initiator DNA only induced a minimal reduction in the transmembrane ionic current. Upon adding the dH_1 and dH_2, the autonomous assembly of the nHCR nanostructures incited highly efficient ionic current blockades. Consequently, the ionic current significantly declined from 12.2×10^{-6} A (the ON state) to 13.1×10^{-8} A (the OFF state), showing a current decrease of almost 99.89%. The ionic current recovered to 9.38×10^{-6} A (the ON state) after treatment with 1 uM dispelling probe Y since the effective channel size was increased. Therefore, the ionic current was higher by nearly 99.86% (Figure 4A). During a previous study, the symmetrical modified HCR assembly was used for the high sensitivity detection of copper ions, while the digestion chains were designed to regenerate the nanochannel.[36] In this work, the nanofluidic gating sensor was constructed based on a universal, sequence Y-induced disassembly of nHCR nanostructures. To improve the realization of the disassembly of the nHCR nanostructure, asymmetric modification was used to modify the DNA nanostructure in only half of the nanochannels. As shown in the inset in Figure 4a, after nHCR assembly, the fabricated nanofluidic gate exhibited both ion current rectification and a high ON−OFF ratio. The ON−OFF ratio was the ratio of the high transmembrane ionic current (OPEN state) and low transmembrane ionic current (CLOSE state) under the same potentials. In this work, a potential of 2 V was chosen to calculate the ON−OFF ratio. The formula for the ON−OFF ratio is list as follows:

ON−OFF ratio = transmembrane ionic current (OPEN state, measured at 2 V)/transmembrane ionic current (CLOSE state, measured at 2 V).

The ON−OFF ratio of the proposed sensor in this study was higher than that of previously reported chemically modified nanofluidic gating systems.[37−39] The high gating effect of the ionic current might be attributed to the good filling properties of nHCR products provided by the flexibility and gradient length of its nanostructures. Following treatment with probe Y, the nHCR nanostructures gradually disassembled due to the extraction of dH2 from the nHCR nanostructures by probe Y_2 to form a new dimer. The digested DNA fragments were easily washed away from the nanochannel, recreating the OPEN nanochannel with high ionic conductivity. As shown in Figure 4B, the ON−OFF ratio

DOI: 10.1021/acs.analchem.9b03489
Anal. Chem. XXXX, XXX, XXX−XXX

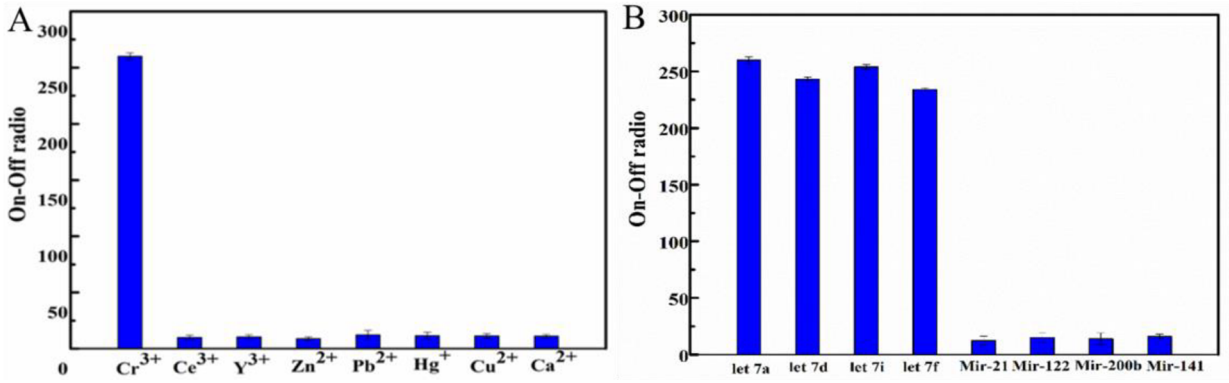

Figure 5. Specificity of the developed nanochannel sensing platform for Cr^{3+} (A) and microRNA (B).

increased as the concentration of Cr^{3+} ions rose from 200 fM to 20 nM, and the microRNA concentration was in the range from 1 pM to 10 nM (Figure 4C). The detection limit for Cr^{3+} and microRNA was as low as 200 fM and 1 pM, respectively.

Specificity of the Nanochannel Sensing Platform. The specificity of the proposed nanochannel biosensor was evaluated by applying various interfering metal ions (Ce^{3+}, Y^{3+}, Zn^{2+}, Pb^{2+}, Hg^{+}, Cu^{2+}, and Ca^{2+}) to the DNAzyme–dEXPAR transformation system. It should be mentioned that the specific cleavage activity of the Ce13d DNAzyme to Cr^{3+} was performed in the presence of 2 mM phosphate[31] since Ce13d DNAzyme displayed 150-fold cleavage activity for the lanthanide ions (Ce^{3+}).[40] Interestingly, inorganic phosphate can sufficiently mask the activity of lanthanide ions, allowing the Ce13d DNAzyme for specific analyzing of Cr^{3+}. As shown in Figure 5A, a high ON–OFF ratio was only obtained in the presence of Cr^{3+} while the ON–OFF ratio for the other interfering metal ions was weak, demonstrating the excellent specificity for detecting Cr^{3+} ions.

To investigate the specific response of the fabricated nanochannel sensor for targeted microRNA, several species of microRNAs were selected to determine the sequence specificity of the proposed sensor. Figure 5B shows that the biosensor cannot differentiate microRNA from the let-7 family, but was highly selective for nonlet-7 family microRNAs.

Reproducibility and Stability. The reproducibility and accuracy of the developed biosensor was determined by investigating five different nHCR assembly identically functionalized nanochannels. A relative standard deviation (RSD) of 12.49% and 9.46% was obtained toward 10 pM Cr^{3+} ions, confirming the high reproducibility and accuracy of the interbiosensor (Tables S4 and S5). Five successive ionic current measurements of one nHCR assembly-functionalized nanochannel for 10 pM Cr^{3+} ion yielded an RSD of 6.28%, indicating good reproducibility of the intrabiosensor (Table S6). The detailed information is listed in the Supporting Information.

The stability of the nHCR assembly-functionalized nanochannel biosensor was also evaluated. The proposed sensor was stored in PBS at 4 °C for a long-term stability study, and the ionic current response to 10 pM Cr^{3+} ions were tested weekly. After a storage period of 1 week, the ionic current of the biosensor decreased by 7.66% compared to the initial response, which indicated moderate stability. After 2 and 3 weeks of storage, the initial ionic current declined by 15.37% and 29.97%, respectively. After 4 weeks of storage, the ionic current remained at 13.78% of its initial response, indicating poor long-term storage stability (Table S7). Therefore, building a fresh nHCR assembly-functionalized nanochannel was recommended for analysis.

CONCLUSION

A sensitive and selective nanochannel sensor for the detection of Cr^{3+} and microRNA is successfully developed by using an easily detachable nHCR nanostructure as a molecular gate inside a nanochannel. In the nanochannel sensor design, a nucleic acid-assisted transformation and amplification system of analytes is also established to expand the target detection range of the nanochannel sensor. The DNAzyme or EXPAR provides the required molecular recognition and imparts selectivity into nonselective nanochannels. The results indicate that the disintegration of the nHCR nanostructure can effectively regulate the electrolyte ion transport inside nanochannels. The developed electrochemical system can sensitively detect the analytes by measuring the ionic current change between the OPEN and CLOSED states of the nanochannel. The developed nanochannel biosensor provides illumination for developing reproducible, environmentally friendly, and complicated multiple target analysis systems in the future.

ASSOCIATED CONTENT

Supporting Information

The Supporting Information is available free of charge on the ACS Publications website at DOI: 10.1021/acs.analchem.9b03489.

Polyacrylamide gel electrophoresis, DNA sequences used in the paper, dispelling probe Y-mediated disassembly, laser scanning confocal microscopy characterization, comparison with other nanochannel-based biosensors, reproducibility and stability, and regeneration of nanochannel biosensor. (PDF)

AUTHOR INFORMATION

Corresponding Author

*Tel/Fax: +86 010 62738793. E-mail: xuwentao@cau.edu.cn.

ORCID

Wentao Xu: 0000-0002-8572-8257

Notes

The authors declare no competing financial interest.

DOI: 10.1021/acs.analchem.9b03489
Anal. Chem. XXXX, XXX, XXX–XXX

■ ACKNOWLEDGMENTS

This work is financially supported by the National Grand Project of Science and Technology (2018ZX08011-06B), the National Natural Science Foundation of China (31801626) and China Postdoctoral Science Foundation (2018M630225).

■ REFERENCES

(1) Hou, X.; Guo, W.; Jiang, L. *Chem. Soc. Rev.* **2011**, *40*, 2385−2401.
(2) Zhang, Z.; Wen, L. P.; Jiang, L. *Chem. Soc. Rev.* **2018**, *47*, 322.
(3) Liu, M. Y.; Zhang, H. C.; Li, K.; Heng, L. P.; Wang, S. T.; Tian, Y.; Jiang, L. *Adv. Funct. Mater.* **2015**, *25*, 421−426.
(4) Zhang, H. C.; Tian, Y.; Jiang, L. *Chem. Commun.* **2013**, *49*, 10048−10063.
(5) Chen, Z. M.; Shen, G. Z.; Li, Y. P.; Zhang, P.; Ji, H. W.; Liu, S. C.; Li, C. Y.; Qian, Z. J. *Electrochem. Commun.* **2015**, *60*, 83−87.
(6) Wang, G. H.; Wang, L.; Han, Y. J.; Zhou, S.; Guan, X. Y. *Biosens. Bioelectron.* **2014**, *53*, 453−458.
(7) Liu, X.; Wei, M.; Liu, Y. J.; Lv, B. J.; Wei, W.; Zhang, Y. J.; Liu, S. Q. *Anal. Chem.* **2016**, *88*, 8107−8114.
(8) Zhao, X. P.; Zhou, Y.; Zhang, Q. W.; Yang, D. R.; Wang, C.; Xia, X. H. *Anal. Chem.* **2019**, *91*, 1185−1193.
(9) Fanzio, P.; Mussi, V.; Menotta, M.; Firpo, G.; Repetto, L.; Guida, P.; Angeli, E.; Magnani, M.; Valbusa, U. *Biosens. Bioelectron.* **2015**, *64*, 219−226.
(10) Shi, L.; Mu, C. L.; Gao, T.; Chai, W. X.; Sheng, A. Z.; Chen, T. S.; Yang, J.; Zhu, X. L.; Li, G. X. *J. Am. Chem. Soc.* **2019**, *141*, 8239.
(11) Gyurcsanyi, R. E. *TrAC, Trends Anal. Chem.* **2008**, *27*, 627−639.
(12) Ikbal, J.; Lim, G. S.; Gao, Z. Q. *TrAC, Trends Anal. Chem.* **2015**, *64*, 86−99.
(13) Dirks, R. M.; Pierce, N. A. *Proc. Natl. Acad. Sci. U. S. A.* **2004**, *101*, 15275−15278.
(14) Wang, J.; Wang, L.; Liu, X.; Liang, Z.; Song, S.; Li, W.; Li, G.; Fan, C. *Adv. Mater.* **2007**, *19*, 3943−3946.
(15) Ying, N.; Ju, C.; Li, Z.; Liu, W.; Wan, J. *Talanta* **2017**, *164*, 432−438.
(16) Wang, Q.; Yang, X.; Yang, X.; Liu, P.; Wang, K.; Huang, J.; Liu, J.; Song, C.; Wang, J. *Spectrochim. Acta, Part A* **2015**, *136*, 283−287.
(17) Quan, K.; Huang, J.; Yang, X.; Yang, Y.; Ying, L.; Wang, H.; He, Y.; Wang, K. *Chem. Commun.* **2015**, *51*, 937.
(18) Zhu, Z.; Lei, J.; Liu, L.; Ju, H. *Analyst* **2013**, *138*, 5995−6000.
(19) Xu, Z.; Yin, H.; Han, Y.; Zhou, Y.; Ai, S. *Anal. Chim. Acta* **2014**, *829*, 9−14.
(20) Song, C.; Xie, G.; Wang, L.; Liu, L.; Tian, G.; Xiang, H. *Biosens. Bioelectron.* **2014**, *58*, 68−74.
(21) Xu, Q.; Zhu, G.; Zhang, C. Y. *Anal. Chem.* **2013**, *85*, 6915−6921.
(22) Oishi, M. *Anal. Bioanal. Chem.* **2015**, *407*, 4165−4172.
(23) Yun, W.; Cai, D.; Jiang, J.; Zhao, P.; Huang, Y.; Sang, G. *Biosens. Bioelectron.* **2016**, *80*, 187−193.
(24) Yang, L.; Liu, C.; Ren, W.; Li, Z. *ACS Appl. Mater. Interfaces* **2012**, *4*, 6450−6453.
(25) Tan, E.; Erwin, B.; Dames, S.; Ferguson, T.; Buechel, M.; Irvine, B.; Voelkerding, K.; Niemz, A. *Biochemistry* **2008**, *47*, 9987−9999.
(26) Ryoo, S. R.; Lee, J.; Yeo, J.; Na, H. K.; Kim, Y. K.; Jang, H.; Lee, J. H.; Han, S. W.; Lee, Y.; Kim, V. N.; Min, D. H. *ACS Nano* **2013**, *7*, 5882−5891.
(27) Wang, J.; Chen, J. Y.; Sen, S. *J. Cell. Physiol.* **2016**, *231*, 25−30.
(28) Vasylkiv, O. Y.; Kubrak, O. I.; Storey, K. B.; Lushchak, V. I. *Chemosphere* **2010**, *80*, 1044.
(29) Zhou, W.; Yu, T.; Vazin, M.; Ding, J.; Liu, J. *Inorg. Chem.* **2016**, *55*, 8193.
(30) Kubrak, O. I.; Lushchak, O. V.; Lushchak, J. V.; Torous, I. M.; Storey, J. M.; Storey, K. B.; Lushchak, V. I. *Comp. Biochem. Physiol., Part C: Toxicol. Pharmacol.* **2010**, *152*, 360−370.
(31) Zhou, W.; Vazin, M.; Yu, T.; Ding, J.; Liu, J. *Chem. - Eur. J.* **2016**, *22*, 9835−9840.
(32) Zhou, W. H.; Saran, R.; Liu, J. W. *Chem. Rev.* **2017**, *117*, 8272−8325.
(33) Li, Z. B.; Miao, X. M.; Xing, K.; Peng, X.; Zhu, A. H.; Ling, L. S. *Biosens. Bioelectron.* **2016**, *80*, 339.
(34) Xu, Q. F.; Zhu, G. C.; Zhang, C. Y. *Anal. Chem.* **2013**, *85*, 6915−6921.
(35) Li, C. X.; Wang, H. Y.; Shen, J.; Tang, B. *Anal. Chem.* **2015**, *87*, 4283−4291.
(36) Abbaspour, A.; Norouz-Sarvestani, F.; Noori, A.; Soltani, N. *Biosens. Bioelectron.* **2015**, *68*, 149−155.
(37) Schepelina, O.; Zharov, I. *Langmuir* **2007**, *23*, 12704−12709.
(38) Swaminathan, V. V.; Gibson, L. R.; Pinti, M.; Prakash, S.; Bohn, P. W.; Shannon, M. A. *J. Nanopart. Res.* **2012**, *14*, na DOI: 10.1007/s11051-012-0951-0.
(39) Guo, W.; Cao, L.; Xia, J.; Nie, F.-Q.; Ma, W.; Xue, J.; Song, Y.; Zhu, D.; Wang, Y.; Jiang, L. *Adv. Funct. Mater.* **2010**, *20*, 1339−1344.
(40) Huang, P. J.; Lin, J.; Cao, J.; Vazin, M.; Liu, J. *Anal. Chem.* **2014**, *86*, 1816−1821.

DOI: 10.1021/acs.analchem.9b03489
Anal. Chem. XXXX, XXX, XXX−XXX